The American Journal of Chinese Medicine, Vol. 49, No. 3, 753–765

DOI: 10.1142/S0192415X2150035X

20(*S*)-Ginsenoside Rg3 Inhibits Lung Cancer Cell Proliferation by Targeting EGFR-Mediated Ras/Raf/MEK/ERK Pathway

Yuan Liang,* Tiehua Zhang,* Siyuan Jing,* Peng Zuo,† Tiezhu Li,†
Yongjun Wang,† Shaochen Xing,† Jie Zhang* and Zhengyi Wei†

**College of Food Science and Engineering, Jilin University*
Changchun 130062, P. R. China
†*Institute of Agricultural Biotechnology, Jilin Academy of Agricultural Sciences*
Changchun 130033, P. R. China

Published 25 February 2021

Abstract: Lung cancer is the leading cause of cancer death in the world and classified into non-small cell lung cancer (NSCLC) and small cell lung cancer (SCLC). As tyrosine kinase inhibitors (TKIs), several triterpenoid saponins can target to epidermal growth factor receptor (EGFR), a widely used molecular therapeutic target, to exhibit remarkable anti-proliferative activities in cancer cells. As one of triterpenoid saponins, 20(*S*)-ginsenoside Rg3 [20(*S*)-Rg3] was confirmed to be an EGFR-TKI in this work. According to the quantitative real-time reverse transcription-PCR (qRT-PCR) and immunoblotting analysis, 20(*S*)-Rg3 was certified to play a key role on EGFR/Ras/Raf/MEK/ERK signal pathway regulation. Our data demonstrated that 20(*S*)-Rg3 might block the cell cycle at the G0/G1 phase by downregulating CDK2, Cyclin A2, and Cyclin E1. Molecular docking suggested that the combination of both hydrophobic and hydrogen-bonding interactions may help stabilizing the 20(*S*)-Rg3-EGFR binding. Furthermore, their binding stability was assessed by molecular dynamics simulation. Taken together, these data provide the evidence that 20(*S*)-Rg3 could prohibit A549 cell proliferation, probably by arresting the cell cycle at the G0/G1 phase via the EGFR/Ras/Raf/MEK/ERK pathway.

Keywords: Epidermal Growth Factor Receptor; 20(*S*)-Ginsenoside Rg3; Cell Proliferation; Cell Cycle; Binding Interaction.

Correspondence to: Dr. Jie Zhang and Dr. Zhengyi Wei, College of Food Science and Engineering, Jilin University, Changchun 130062, P. R. China. Tel: (+86) 431-8783-6361, Fax: (+86) 431-8783-6361, E-mail: zhangjie83@jlu.edu.cn (J. Zhang); Institute of Agricultural Biotechnology, Jilin Academy of Agricultural Sciences, Changchun 130033, P. R. China. Tel: (+86) 431-8706-3127, Fax: (+86) 431-8706-3200, E-mail: weizy80@163.com (Z. Wei)

Introduction

Lung cancer is the main cause of cancer death worldwide, while it is classified into two major groups, non-small cell lung cancer (NSCLC), and small cell lung cancer (SCLC) (Hsu *et al*., 2004). As a NSCLC cell line, A549 cell shows significantly higher expression of lung-resistance protein (LRP) than other lung cancer cell lines (Lin *et al*., 2009). As the current treatment modalities are inadequate, novel therapies are necessary to reduce the impacts of increased lung cancer incidence rate.

Epidermal growth factor receptor (EGFR) is often considered as a molecular therapeutic target because of its overexpression in lung tumors (Liang *et al*., 2020; Zhang *et al*., 2020a). Binding of epidermal growth factor (EGF) induces EGFR dimerization and phosphorylation, which leads to the activation of downstream signaling pathways, such as RAS/RAF/MEK/ERK, PI3K/AKT/mTOR, and JAK/STAT3 pathways (Bansode *et al*., 2018). Considering the therapeutic therapy targeting EGFR, there are two well-identified varieties of drugs, including epidermal growth factor receptor-tyrosine kinase inhibitors (EGFR-TKIs) and monoclonal antibodies (mAbs) (Lin *et al*., 2014; Jing *et al*., 2020b). However, treatment with the synthetic EGFR-TKIs is associated with several side effects, such as rash and diarrhea (Hu *et al*., 2017; Jing *et al*., 2020a). Thus, searching for novel EGFR-TKIs with more effective and less side effects is urgently needed.

As one of the classical traditional Chinese medicines (TCMs), *Panax ginseng* (*P. ginseng*) can inhibit the proliferation of tumor cells and produce little relative toxicity to normal cells, making it an attractive candidate for cancer treatment (Zhang *et al*., 2018; Xiao *et al*., 2019). Ginsenosides are the main active ingredients in *P. ginseng* and are mainly derived from the root (Ren *et al*., 2019; Zhang *et al*., 2020d). The absence or presence of the carboxyl group at the C-6 position can divide ginsenosides into two categories, namely, protopanaxatriol (PPT)-type and protopanaxadiol (PPD)-type (Zhang *et al*., 2020c). Rg3 is one of the bioactive PPD-type ginsenosides and has been developed as a potential natural anticancer substance in Asian countries (Zhang *et al*., 2019b). It exists as a pair of stereoisomers, 20(*S*)-ginsenoside Rg3 [20(*S*)-Rg3], and 20(*R*)-ginsenoside Rg3 [20(*R*)-Rg3], depending on the spatial arrangement of the hydroxyl group at C-20 (Zhang *et al*., 2019c; Li *et al*., 2020).

It has been reported that 20(*S*)-Rg3 (Fig. 1A) is more water soluble and bioavailable than its 20(*R*) counterpart (Tian *et al*., 2016; Wang *et al*., 2019). Hence, this work investigated the effect of 20(*S*)-Rg3 on the regulation of cell proliferation in A549 cells. First, 20(*S*)-Rg3 was proved to be an EGFR kinase inhibitor by the homogeneous time-resolved fluorescence (HTRF) method. The influence of 20(*S*)-Rg3 to A549 cells growth and viability was evaluated by MTT assay. The results also confirmed that 20(*S*)-Rg3 could regulate the expression of EGFR/MAPK pathway genes as well as the level of relative proteins in A549 cells. Further investigation suggested that 20(*S*)-Rg3 probably could block the cells cycle but not regulate apoptosis in A549 cells. In addition, the binding interaction between EGFR and 20(*S*)-Rg3 was investigated by molecular docking in combination with molecular dynamics (MD) simulation.

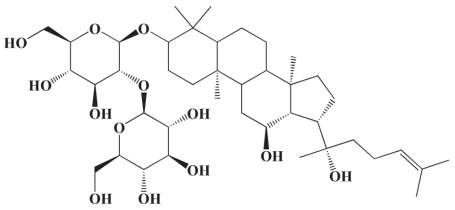

(A)

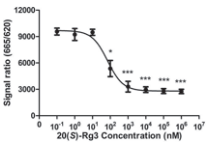

(B)

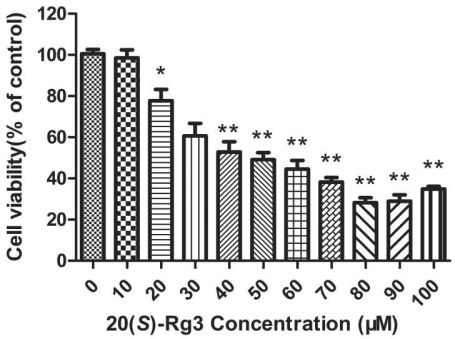

(C)

Figure 1. (A) The structure of 20(*S*)-Rg3. (B) The inhibition assay of 20(*S*)-Rg3 to EGFR kinase. The inhibition curve was calculated with the ratio at 620 and 665 nm on a microplate reader. (C) The MTT assay was performed to determine the A549 cells cytotoxicity following 24 h exposure to different concentrations of 20(*S*)-Rg3. The assays were repeated independent three times and all the data were presented as mean ± SEM. $^{*}P < 0.05$, $^{**}P < 0.01$, and $^{***}P < 0.001$ compared with the control group.

Materials and Methods

Materials

20(*S*)-Rg3 was purchased from Yuanye Biotech Co., Ltd. (Shanghai, China). Dulbecco's modified Eagle's medium (DMEM), phosphate-buffered saline (PBS), and trypsin-ethylene diamine tetraacetie acid (EDTA) solution were purchased from Biological Industries (Beit Haemek, Israel). Antibiotic solution containing 1×10^4 U/mL penicillin and 1×10^4 μg/mL streptomycin was purchased from Gibco (Paisley, UK). Fetal bovine serum (FBS) was purchased from HyClone (South Logan, USA). Primary antibodies were purchased from Abcam (Cambridge, USA). Glyceraldehyde-3-phosphate dehydrogenase (GAPDH) antibody was purchased from Gene Tex (Irvine, CA, USA). Horseradish peroxidase (HPR)-conjugated secondary antibody was purchased from Sino Biological Inc. (Beijing, China).

EGFR HTRF Assay

The kinase inhibition assay for the EGFR protein (Thermo Fisher Scientific, San Jose, USA) was performed using the HTRF kinase TK assay kit (Cisbio, Codolet, France). Briefly, the enzyme reaction was carried out with the addition of ATP to a mixture of 20(*S*)-Rg3, TK substrate-biotin, and EGFR protein. The EGFR enzyme reaction was performed at room temperature for 40 min and was terminated by the detection buffer containing EDTA with streptavidin and TK antibody-cryptate (Zhang *et al*., 2019a). Then the 96-well low volume plate was read at 620 and 665 nm on a microplate

reader (Tecan Spark® 10M, Tecan, Männedorf, Switzerland). The competition curve of 20(*S*)-Rg3 to EGFR kinase was fitted with the GraphPad Prism 5 (GraphPad Software, La Jolla, USA).

Cell Lines and Culture

A549 cell was purchased from Cell Bank of Chinese Academy of Sciences (Shanghai, China). The A549 cells were maintained in DMEM supplemented with 100 U/mL penicillin, 100 μg/mL streptomycin, and 10% FBS in the humidified atmosphere with 95% air and 5% CO_2 at 37 °C.

Proliferation Assay

The effect of 20(*S*)-Rg3 on A549 cells proliferation and viability was assessed by MTT assay kit (Sigma-Aldrich, St. Louis, USA). A549 cells were cultured in 96-well plates at 1×10^4 cells per well for 24 h. Then cells were treated with 20(*S*)-Rg3 at different concentrations. After 24 h treatment of 20(*S*)-Rg3, MTT solution (5 mg/mL) was added into each experiment well and cells were incubated at 37 °C. Another 4 h later, the DMEM medium was discarded, and 110 μL of DMSO was added to dissolve the formazan in A549 cells. The absorbance changes at 490 nm were detected with a microplate reader (Bio-Rad Laboratories, Richmond, USA).

Quantitative Real-Time PCR Assay

The distinct genes were verified by quantitative real-time reverse transcription-PCR (qRT-PCR). The A549 cells were precultured in DMEM medium of 2.5×10^5 cells per disc for about 12 h. Different concentrations of 20(*S*)-Rg3 were added to cells for 24 h, then total cellular RNA of samples was extracted from the 549 cells with the Trizol reagent (Transgen Biotech Ltd., Beijing, China) on the basis of manufacturer's protocol. The cDNA was synthesized from the mRNA with a PrimeScript® RT reagent kit (Transgen Biotech Ltd., Beijing, China). On the basis of the primer sequences (Zhang *et al*., 2020b), the qRT-PCR was performed with Step One Plus® RT-PCR system (Applied Biosystems, Forster City, USA). GAPDH was used as an internal control. Relative expression level of the genes was calculated by using the $^{\Delta\Delta}$Ct method, and the values less than 0.5 or greater than 2.0 were considered as significantly down- or up-regulated.

Western Blotting

The cells were cultured at 5×10^6 cells per disc in 10 cm discs. After attachment, cells were treated with 20(*S*)-Rg3 for 24 h. Then cells were washed twice or three times with ice-cold PBS and were scraped into radio-immunoprecipitation assay (RIPA) buffer. Cell lysates were incubated for about 30 min on ice. After being centrifugated at 12,000 g for 5 min, the supernatant was taken as protein solution. The concentration of protein was detected with

a bicinchoninic acid (BCA) protein assay kit (Melunbio, Dalian, China). Protein samples were assessed by sodium dodecyl sulfate-poly acrylamide gel electrophoresis (SDS-PAGE) and were electroblotted onto polyvinylidene fluoride (PVDF) membranes. After blocking of non-specific binding, the expressions of proteins were estimated. GAPDH was used as an internal control. After washing with TBST buffer several times at room temperature, the PVDF membranes were incubated by secondary antibodies with continuous shaking. The proteins expressions were detected with an enhanced chemiluminescence testing kit (Clinx Science Instrument Co., Ltd., Shanghai, China). The gray densities of the bands were measured with ImageJ program (Softonic International S.A.). Relative accumulation of the tested proteins was calculated by using the gray density values referred to those of the GAPDH in the same treatments.

Computer Simulation and Analysis

Initially, the co-crystal structure of EGFR-erlotinib complex (Protein Data Bank ID 1M17) was collected (Stamos *et al*., 2002). After the validation of docking accuracy, EGFR and 20(*S*)-Rg3 were submitted to AutoDockTools for 10 independent docking calculations. The docking pose with lowest binding energy was selected as the best pose for the MD simulation. Briefly, the 20(*S*)-Rg3-EGFR complex was located in a cubic box with the simple point charge water models. Then the counterion was placed at random position among the water molecules to obtain electrostatic neutrality. After energy minimization, the system was equilibrated with position restraints on both EGFR and 20(*S*)-Rg3. The position restraints were removed and then MD simulation was performed with GROMACS 2019 for 20 ns. The root mean squared deviation (RMSD) values of 20(*S*)-Rg3 and EGFR were calculated, respectively.

Statistical Analysis

Data were reported as mean ± standard errors of the means (SEM) of the three independent experiments. Statistical significance analysis was performed by the student's *t*-test compared to the control group. The differences were considered significantly for * $P < 0.05$, ** $P < 0.01$, and *** $P < 0.001$.

Results and Discussion

20(S)-Rg3 is an EGFR Kinase Inhibitor

In the HTRF assay, the fluorescence resonance energy transfer signals are generated between the donor and acceptor molecules in close proximities (Wang *et al*., 2014). The media interference is also obviously reduced by dual-wavelength detection. Therefore, the HTRF assay is widely performed in the kinase assays that mainly focus on the high-throughput screening. The HTRF method was arranged to evaluate the inhibitory activity of 20(*S*)-Rg3

to EGFR kinase. The inhibition curve of 20(*S*)-Rg3 was shown in Fig. 1B. The half maximal inhibitory concentration (IC_{50}) value of 20(*S*)-Rg3 inhibiting wild-type EGFR kinase was 70.42 nM. Therefore, the HTRF assay results confirmed that 20(*S*)-Rg3 was an EGFR kinase inhibitor and might be a potential therapy in the treatment of NSCLC.

Cytotoxicity of 20(S)-Rg3 to A549 Cells

The MTT analysis was carried out to determine the A549 cells cytotoxicity following 24 h exposure to different concentrations of 20(*S*)-Rg3. The results indicated that 20(*S*)-Rg3 could inhibit A549 cells viability in a dose-dependent manner and the cell viability was basically stable after the treatment of 20(*S*)-Rg3 at about 50 μM (Fig. 1C). The concentrations of 24, 30, and 37 μM were selected for further cell treatments, corresponding with the IC_{20}, IC_{40}, and IC_{60} in A549 cells, respectively.

20(S)-Rg3 Regulated the EGFR/MAPK Signaling in A549 Cells

To investigate whether the EGFR/MAPK signaling is regulated by 20(*S*)-Rg3, both of qRT-PCR and western blotting analysis were carried out. Obviously, the expressions of the EGFR/MAPK pathway genes were regulated in a concentration-dependent manner with the increased concentration levels of 20(*S*)-Rg3, except for that of *ERK1* (Fig. 2A). In all treatments, the expression of Ras was significantly upregulated. High concentration (37 μM) of 20(*S*)-Rg3 significantly upregulated the expressions of *EGFR*, *BRAF*, *MEK2*, and *ERK2*. However, only the expressions of *Ras*, *BRAF*, and *MEK2* were remarkably upregulated when treated with moderate concentration (30 μM) of 20(*S*)-Rg3. Interestingly, the expressions of *Raf1*, *ERK1*, and *ERK2* were remarkably downregulated when treated with low concentration (24 μM) of 20(*S*)-Rg3. Hence, it could be concluded that the high concentration of 20(*S*)-Rg3 promoted the expressions of genes in EGFR/

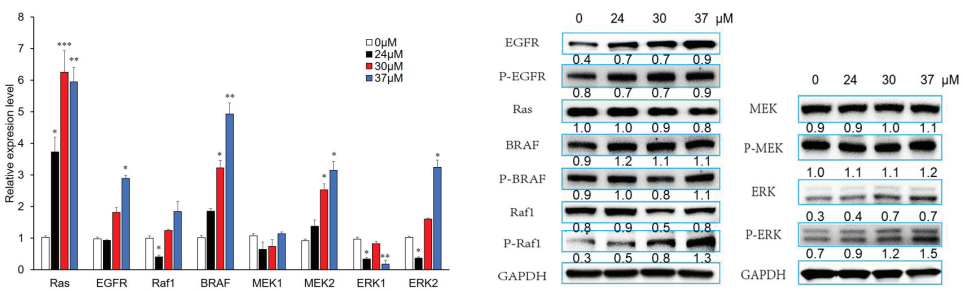

(A) (B)

Figure 2. Regulation of 20(*S*)-Rg3 to EGFR/MAPK pathway. (A) Gene expression data were achieved from three independent technical duplicates with three independent treatments. (B) Cells lysates were probed with antibodies to detect the correspondent proteins. The numbers under bands indicated the relative accumulation levels. The assays were repeated independent three times and all the data were presented as mean ± SEM. **P* < 0.05, ***P* < 0.01, and ****P* < 0.001 compared with the control group.

MAPK pathway in A549 cells. The proteins levels of EGFR, ERK, phosphorylated Raf1, and phosphorylated ERK were increased in a concentration-dependent manner (Fig. 2B). Oppositely, both of Ras and Raf1 were decreased as the concentrations of 20(*S*)-Rg3 increased. However, the levels of phosphorylated EGFR and BRAF were increased but not in a concentration-dependent manner. By contrast, the levels of MEK and phosphorylated MEK were basically unchanged with the treatment of 20(*S*)-Rg3 at different concentrations. These results indicated that 20(*S*)-Rg3 could regulate the EGFR/MAPK signaling in A549 cells. The disaccords of transcription and protein accumulation of some tested protein (e.g., Ras and Caspase-3 described below) might be caused by the post transcription processing/modification of mRNAs and/or translation regulation as well as the degradation of the proteins.

20(S)-Rg3 Did Not Inhibit A549 Cells Apoptosis

Apoptosis is a constitutive, active, and energy-dependent process that is performed by a number of characteristics, such as cytoplasmic shrinkage, active membrane blebbing, nuclear condensation, internucleosomal DNA fragmentation, and protein cleavage (Orrenius *et al*., 2011). As shown in Fig. 3A, the expressions of the apoptosis-related genes (*Caspase-3*, *STAT3*, and *survivin*) were upregulated in a concentration-dependent manner. However, the expressions of *PARP1*, *Caspase-9*, and *Bcl-XL* reached their highest level at moderate concentration (30 μM) of 20(*S*)-Rg3. The results of the western blotting analysis showed that PARP1 decreased in a concentration-dependent manner, while phosphorylated STAT3 increased (Fig. 3B). Interestingly, the level of survivin was remarkably increased at high concentration (37 μM) of 20(*S*)-Rg3. However, the levels of STAT3, Caspase-9, Caspase-3, and Bcl-XL were basically unchanged with the treatment of 20(*S*)-Rg3 at the tested concentrations.

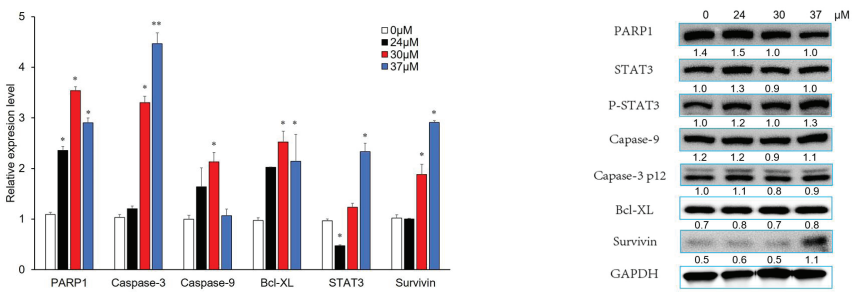

Figure 3. Impacts of 20(*S*)-Rg3 to apoptosis regulators. (A) Gene expression data were achieved from three independent technical duplicates with three independent treatments. (B) Cells lysates were probed with antibodies to detect the correspondent proteins. The numbers under bands indicated the relative accumulation levels. The assays were repeated independently three times and all the data were presented as mean ± SEM. $*P < 0.05$, $**P < 0.01$, and $***P < 0.001$ compared with the control group.

As the most abundant isoform of the PARP enzyme family, PARP1 plays a key role as DNA damage sensor and signaling molecule by binding to both single- and double-stranded DNA breaks (Xu *et al*., 2016). The downregulation of PARP1 induced by 20(*S*)-Rg3 made A549 cells vulnerable to death. STAT proteins are potential transcription factors that mediate growth factor- and cytokine-directed transcription. *STAT3* is persistently activated in many transformed cell lines and human cancers, therefore *STAT3* is considered as an oncogene (Darnell, 2002). The reduction of PARP1 level could increase A549 cells apoptosis, however the increment of phosphorylated STAT3 level could promote cancer cells proliferation. In this work, the influence of the downregulation of PARP1 cancelled out that of the increment of phosphorylated STAT3, resulting in the constant level of other apoptosis-related proteins and their phosphorylation. As one of the anti-apoptosis genes, *survivin* is validated as the cancer therapeutic target. The overexpression of survivin was widely identified to be a negative prognostic factor in different cancer types and participated in the inhibition of apoptosis by anticancer agents (Altieri, 2008). At high concentrations, the increment of survivin level was probably affected by the phosphorylated STAT3. Therefore, 20(*S*)-Rg3 might not induce A549 cell apoptosis.

20(S)-Rg3 Blocked the Cell Cycle at the G0/G1 Phase

Cell division is divided into mitosis (M) and interphase (includes G1, S, and G2 phases) according to the characterization of replicated DNA and segregation of replicated chromosomes (Vermeulen *et al*., 2003). Generally speaking, most of the expressions of the cell cycle-related genes were significantly upregulated by moderate concentration (30 μM) of 20(*S*)-Rg3, except for that of *CDK1* and *Cyclin B1* (Fig. 4A). In all cases, the expressions of *Cdc25C*, *CDK2*, *CDK4*, and *p53* were all significantly upregulated. By contrary, *RSK1* and *Cyclin A2* were downregulated at high concentration (37 μM) of 20(*S*)-Rg3, while *Cyclin B1* was downregulated at both 24 and 30 μM of 20(*S*)-Rg3. As for the protein aspect, the levels of phosphorylated proteins such as Cdc25A, Cyclin A2, Cyclin B1, Cyclin E1, and CDK2 were all decreased (Fig. 4B). The level of RSK1 was decreased, while the level of phosphorylated RSK was increased. Interestingly, the levels of both Cdc25C and phosphorylated Cdc25C were increased. However, the levels of Cyclin D1, CDK1, phosphorylated CDK1/2, and CDK4 were basically unchanged. The levels of both p53 and phosphorylated p53 were increased.

As cell cycle regulators, the CDK2-Cyclin E complex completes retinoblastoma protein phosphorylation, thereby allowing for entering into the S phase. Subsequently, the complex formation of CDK2-Cyclin A will cause phosphorylation of proteins in DNA replication (Verbon *et al*., 2012). The decreased proteins levels of CDK2 and Cyclin E1 inhibited the cell cycle transition through G1 phase to DNA synthesis S phase, therefore arrested the A549 cells at G0/G1 phase. Indeed, CDK2-Cyclin A also plays a key factor in the initiation of centrosome duplication. As one of the tumor suppressor proteins, the function of p53 is a regulator of transcription. It is proposed that p53 could modulate both mitochondria-dependent and mitochondria-independent apoptotic pathways (He *et al*., 2011). The upregulation of p53 contributed to the DNA-damage-induced cell death (Gao *et al*., 2011). In this

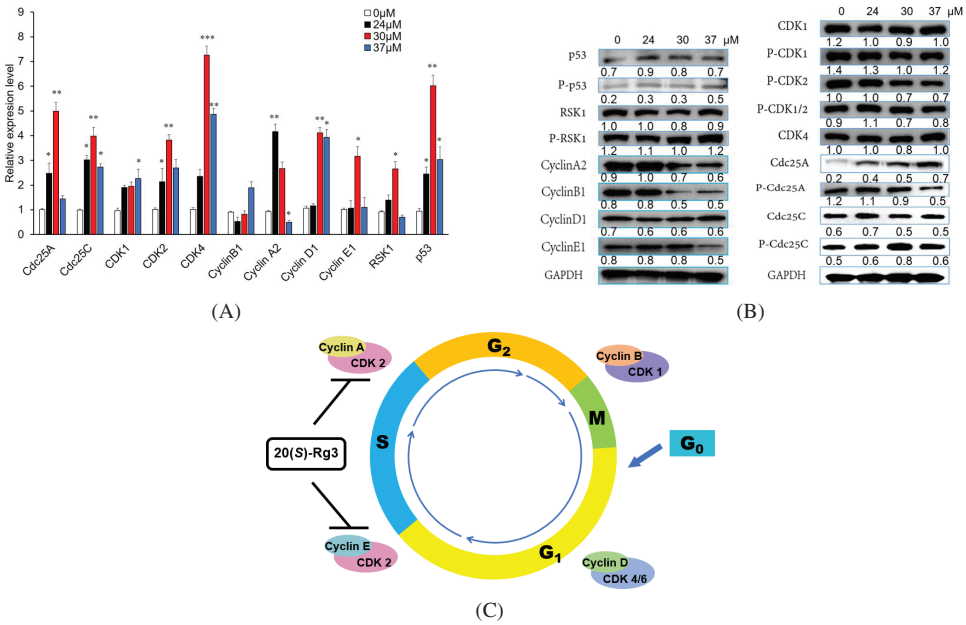

Figure 4. Impacts of 20(*S*)-Rg3 to cell cycle regulators. (A) Gene expression data were achieved from three independent technical duplicates with three independent treatments. (B) Cells lysates were probed with antibodies to detect the correspondent proteins. The numbers under bands indicated the relative accumulation levels. (C) Schematic of the cell cycle progression. 20(*S*)-Rg3 could decrease the proteins expressions including CDK2, Cyclin A2, and Cyclin E1, as well as block the progression of cell cycle at the G0/G1 phase. The assays were repeated independently three times and all the data were presented as mean ± SEM. $*P < 0.05$, $**P < 0.01$, and $***P < 0.001$ compared with the control group.

study, our data demonstrated that 20(*S*)-Rg3 could inhibit the progression of cell cycle and decrease the proteins expressions including CDK2, Cyclin A2, and Cyclin E1 (Fig. 4C). These data suggested that cell cycle may be blocked at the G0/G1 phase.

Binding Interaction between EGFR and 20(S)-Rg3

In this work, molecular docking was first performed to investigate the binding conformation of 20(*S*)-Rg3 in the tyrosine kinase domain of EGFR. As shown in Fig. 5A, the sugar moiety consisting of two glucoses at C-3 fits into the hydrophobic region and occupies the ATP-binding site. However, the steroid skeleton of 20(*S*)-Rg3 combined with the sugar moiety at C-20 is too large to be accommodated within this binding pocket. The results of molecular docking indicate that the binding between EGFR and 20(*S*)-Rg3 depends mainly on the contribution of both hydrophobic and hydrogen-bonding interactions. The amino acid residues of EGFR that lie within 4 Å away from 20(*S*)-Rg3 can be observed in Fig. 5B. Among which, Val693, Leu694, Phe699, Val702, Ala719, Met742, Leu768, Met769, Pro770, Phe771, and Leu820 make extensive hydrophobic interactions with

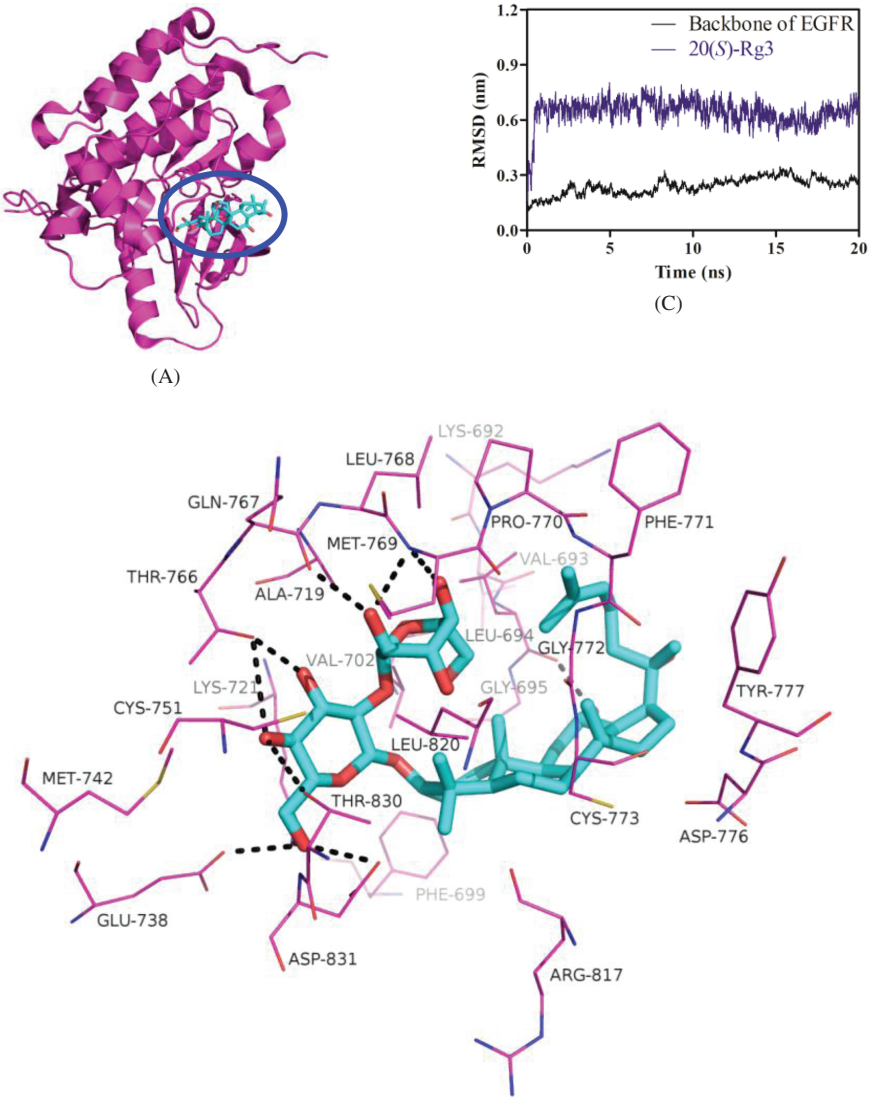

Figure 5. The results of molecular docking (A and B) and molecular dynamics simulation (C) between 20(*S*)-Rg3 and EGFR. Black dashed lines, hydrogen bonds.

20(*S*)-Rg3. Along with these hydrophobic interactions, multiple hydrogen-bonding interactions also seem to be important in stabilizing 20(*S*)-Rg3-EGFR binding. As shown in Fig. 5B, 20(*S*)-Rg3 makes hydrogen-bonding interactions with Leu694, Lys721, Glu738, Thr766, Gln767, Met769, Thr830, and Asp831, thus helping stabilize the position of 20(*S*)-Rg3 in the ATP-binding site. It is remarkable that both of Leu694 and Met769 play a crucial role in 20(*S*)-Rg3 binding to EGFR, providing hydrogen bonding as well

as hydrophobic interaction, which is consistent with previously published studies (Singh and Bast, 2014).

Then, the molecular dynamics simulation was performed to evaluate the binding stability of 20(*S*)-Rg3 with EGFR. As shown in Fig. 5C, the backbone of EGFR basically maintains equilibrium throughout the whole 20 ns simulation process with an average RMSD value of 0.24 ± 0.05 nm. By contrast, 20(*S*)-Rg3 undergoes a drastic conformational change in the initial stage and then maintains equilibrium after approximately 0.5 ns with average RMSD value of 0.64 ± 0.07 nm. As shown in Fig. 5A, the steroid skeleton of 20(*S*)-Rg3 combined with the sugar moiety at C-20 protrudes out of the hydrophobic region and is incapable of stabilizing its conformation. This binding mode may serve to explain the more conformation fluctuation of 20(*S*)-Rg3 compared with EGFR.

Basically speaking, inhibition of tyrosine kinases by TKIs does not directly affect to the mRNA accumulation of the corresponding tyrosine kinases but the demands of the tyrosine kinases in the relative biological processes might feedback to the transcription switches of the tyrosine kinases though various signaling pathways, thus upregulate the expression of the corresponding genes. Thereby, the expression variation was observed as mentioned above.

Conclusion

HTRF assay indicated that 20(*S*)-Rg3 was a potential EGFR-TKI and could inhibit the proliferation of A549 cells. The expressions of genes and corresponding proteins levels in the EGFR/MAPK pathway were regulated after the treatment of 20(*S*)-Rg3. Apoptosis-related genes such as *PARP1*, *STAT3*, and *survivin* were upregulated. On the other aspect, accumulation of PARP1 was decreased while the phosphorylated STAT3 and survivin were increased. However, the other genes and their respective proteins remained relatively constant. These tendencies indicated that 20(*S*)-Rg3 could not induce apoptosis. As for cell cycle-related genes, treatment of 20(*S*)-Rg3 significantly upregulated the expressions of *CDK2*, *Cyclin A2*, and *Cyclin E1*, but the respective proteins CDK2, Cyclin A2, and Cyclin E1 decreased in a concentration-dependent manner. These tendencies suggested that cell cycle might be blocked at the G0/G1 phase. On this basis, the binding interaction of 20(*S*)-Rg3 with EGFR was investigated by computer simulation and analysis. Molecular docking suggested that both hydrophobic and hydrogen-bonding interactions contribute to stabilizing the 20(*S*)-Rg3-EGFR binding. Furthermore, their binding stability was assessed by determining the RMSD values of 20(*S*)-Rg3 and EGFR. In conclusion, 20(*S*)-Rg3 could inhibit A549 cell proliferation and probably arrest cell cycle in A549 cells via the EGFR/Ras/Raf/MEK/ERK pathway.

Acknowledgments

This work was supported by the National Natural Science Foundation of China (31871717, 31972160, and U19A2035), the National Key Research and Development Program of

China (2018YFD0300201), the Science and Technology Development Project Foundation of Jilin Province (20200201204JC), the Agricultural Science and Technology Innovation Program of Jilin Province (CXGC2017TD004), and the Ph.D. Interdisciplinary Research Funding Project of Jilin University (101832020DJX054).

References

Altieri, D.C. Survivin, cancer networks and pathway-directed drug discovery. *Nat. Rev. Cancer* 8: 61–70, 2008.

Bansode, R.R., N.J. Plundrich, P.D. Randolph, M.A. Lila and L.L. Williams. Peanut flour aggregation with polyphenolic extracts derived from peanut skin inhibits IgE binding capacity and attenuates RBL-2H3 cells degranulation via MAPK signaling pathway. *Food Chem*. 263: 307–314, 2018.

Darnell, J.E. Transcription factors as targets for cancer therapy. *Nat. Rev. Cancer* 2: 740–749, 2002.

Gao, W., Z. Shen, L. Shang and X. Wang. Upregulation of human autophagy-initiation kinase ULK1 by tumor suppressor p53 contributes to DNA-damage-induced cell death. *Cell Death Differ*. 18: 1598–1607, 2011.

He, Z.-Y., C.-B. Shi, H. Wen, F.-L. Li, B.-L. Wang and J. Wang. Upregulation of p53 expression in patients with colorectal cancer by administration of curcumin. *Cancer Invest*. 29: 208–213, 2011.

Hsu, Y.-L., P.-L. Kuo, C.-F. Liu and C.-C. Lin. Acacetin-induced cell cycle arrest and apoptosis in human non-small cell lung cancer A549 cells. *Cancer Lett*. 212: 53–60, 2004.

Hu, Y., Z. Li, L. Wang, L. Deng, J. Sun, X. Jiang, Y. Zhang, L. Tian, Y. Wang and W. Bai. Scandenolone, a natural isoflavone derivative from Cudrania tricuspidata fruit, targets EGFR to induce apoptosis and block autophagy flux in human melanoma cells. *J. Funct. Foods* 37: 229–240, 2017.

Jing, S.-Y., Z.-D. Wu, T.-H. Zhang, J. Zhang and Z.-Y. Wei. *In vitro* antitumor effect of cucurbitacin E on human lung cancer cell line and its molecular mechanism. *Chin. J. Nat. Medicines* 18: 483–490, 2020a.

Jing, S., H. Zou, Z. Wu, L. Ren, T. Zhang, J. Zhang and Z. Wei. Cucurbitacins: Bioactivities and synergistic effect with small-molecule drugs. *J. Funct. Foods* 72: 104042, 2020b.

Li, W., J.Q. Wang, Y.D. Zhou, J.G. Hou, Y. Liu, Y.P. Wang, X.J. Gong, X.H. Lin, S. Jiang and Z. Wang. Rare Ginsenoside 20(R)-Rg3 inhibits d-galactose-induced liver and kidney injury by regulating oxidative stress-induced apoptosis. *Am. J. Chin. Med*. 48: 1141–1157, 2020.

Liang, Y., T. Zhang and J. Zhang. Natural tyrosine kinase inhibitors acting on the epidermal growth factor receptor: Their relevance for cancer therapy. *Pharrmacol. Res*. 161: 105164, 2020.

Lin, S.-S., K.-C. Lai, S.-C. Hsu, J.-S. Yang, C.-L. Kuo, J.-P. Lin, Y.-S. Ma, C.-C. Wu and J.-G. Chung. Curcumin inhibits the migration and invasion of human A549 lung cancer cells through the inhibition of matrix metalloproteinase-2 and -9 and vascular endothelial growth factor (VEGF). *Cancer Lett*. 285: 127–133, 2009.

Lin, Y., X. Wang and H. Jin. EGFR-TKI resistance in NSCLC patients: Mechanisms and strategies. *Am. J. Cancer Res*. 4: 411–435, 2014.

Orrenius, S., P. Nicotera and B. Zhivotovsky. Cell death mechanisms and their implications in toxicology. *Toxicol. Sci*. 119: 3–19, 2011.

Ren, S., J. Leng, X.Y. Xu, S. Jiang, Y.P. Wang, X.T. Yan, Z. Liu, C. Chen, Z. Wang and W. Li. Ginsenoside Rb1, a major saponin from *Panax ginseng*, exerts protective effects against acetaminophen-induced hepatotoxicity in mice. *Am. J. Chin. Med*. 47: 1815–1831, 2019.

Singh, P. and F. Bast. In silico molecular docking study of natural compounds on wild and mutated epidermal growth factor receptor. *Med. Chem. Res*. 23: 5074–5085, 2014.

Stamos, J., M.X. Sliwkowski and C. Eigenbrot. Structure of the epidermal growth factor receptor kinase domain alone and in complex with a 4-anilinoquinazoline inhibitor. *J. Biol. Chem*. 277: 46265–46272, 2002.

Tian, L., D. Shen, X. Li, X. Shan, X. Wang, Q. Yan and J. Liu. Ginsenoside Rg3 inhibits epithelial-mesenchymal transition (EMT) and invasion of lung cancer by down-regulating FUT4. *Oncotarget* 7: 1619–1632, 2016.

Verbon, E.H., J.A. Post and J. Boonstra. The influence of reactive oxygen species on cell cycle progression in mammalian cells. *Gene* 511: 1–6, 2012.

Vermeulen, K., D.R. Van Bockstaele and Z.N. Berneman. The cell cycle: A review of regulation, deregulation and therapeutic targets in cancer. *Cell Prolif*. 36: 131–149, 2003.

Wang, X.-J., R.-J. Zhou, N. Zhang and Z. Jing. 20(S)-ginsenoside Rg3 sensitizes human non-small cell lung cancer cells to icotinib through inhibition of autophagy. *Eur. J. Pharmacol*. 850: 141–149, 2019.

Wang, Z., S. Lin, D. Wang and L. Huang. Anti-epidermal growth factor receptor tyrosine kinase activities of traditional Chinese medicine for cancer treatment. *Eur. J. Integr. Med*. 6: 565–570, 2014.

Xiao, H., Q. Xue, Q. Zhang, C. Li, X. Liu, J. Liu, H. Li and J. Yang. How ginsenosides trigger apoptosis in human lung adenocarcinoma cells. *Am. J. Chin. Med*. 47: 1737–1754, 2019.

Xu, F.-Y., W.-Q. Shang, J.-J. Yu, Q. Sun, M.-Q. Li and J.-S. Sun. The antitumor activity study of ginsenosides and metabolites in lung cancer cell. *Am. J. Transl. Res*. 8: 1708–1718, 2016.

Zhang, J., Y. Song, Y. Liang, H. Zou, P. Zuo, M. Yan, S. Jing, T. Li, Y. Wang, D. Li, T. Zhang and Z. Wei. Cucurbitacin IIa interferes with EGFR-MAPK signaling pathway leads to proliferation inhibition in A549 cells. *Food Chem. Toxicol*. 132: 110654, 2019a.

Zhang, T., Y. Liang and J. Zhang. Natural and synthetic compounds as dissociated agonists of glucocorticoid receptor. *Pharrmacol. Res*. 156: 104802, 2020a.

Zhang, T., Y. Liang, P. Zuo, S. Jing, T. Li, Y. Wang, C. Lv, D. Li, J. Zhang and Z. Wei. 20(S)-Protopanaxadiol blocks cell cycle progression by targeting epidermal growth factor receptor. *Food Chem. Toxicol*. 135: 111017, 2020b.

Zhang, T., Y. Liang, P. Zuo, M. Yan, S. Jing, T. Li, Y. Wang, J. Zhang and Z. Wei. Identification of 20(R, S)-protopanaxadiol and 20(R, S)-protopanaxatriol for potential selective modulation of glucocorticoid receptor. *Food Chem. Toxicol*. 131: 110642, 2019b.

Zhang, T., S. Zhong, L. Hou, Y. Wang, X. Xing, T. Guan, J. Zhang and T. Li. Computational and experimental characterization of estrogenic activities of 20(S, R)-protopanaxadiol and 20(S, R)-protopanaxatriol. *J. Ginseng Res*. 44: 690–696, 2020c.

Zhang, T., S. Zhong, T. Li and J. Zhang. Saponins as modulators of nuclear receptors. *Crit. Rev. Food Sci. Nutr*. 60: 94–107, 2020d.

Zhang, T., S. Zhong, Y. Wang, S. Dong, T. Guan, L. Hou, X. Xing, J. Zhang and T. Li. *In vitro* and in silico perspectives on estrogenicity of tanshinones from Salvia miltiorrhiza. *Food Chem*. 270: 281–286, 2019c.

Zhang, X.-W., W. Liu, H.-L. Jiang and B. Mao. Chinese herbal medicine for advanced non-small-cell lung cancer: A systematic review and meta-analysis. *Am. J. Chin. Med*. 46: 923–952, 2018.